Solar Physics (2006) 239: 317–335
DOI: 10.1007/s11207-006-0177-3

THE MAY 13, 2005 ERUPTION: OBSERVATIONS, DATA ANALYSIS AND INTERPRETATION

V. YURCHYSHYN
Big Bear Solar Observatory, Big Bear City, CA 92314, USA

C. LIU
Center for Solar Research of New Jersey Institute of Technology, Newark, NJ 07102, USA

V. ABRAMENKO
Big Bear Solar Observatory, Big Bear City, CA 92314, USA

and

J. KRALL
Plasma Physics Division, Naval Research Laboratory, Washington, DC 20375-5000, USA

(Received 17 March 2006; accepted 31 October 2006; Published online 30 November 2006)

Abstract. In this study, we present detailed description and analysis of the May 13, 2005 eruption, the corresponding coronal mass ejection (CME) and intense geomagnetic storm observed near the Earth on May 15, 2005. This isolated two-ribbon M8.0 flare and the very fast CME occurred in a relatively simple magnetic configuration during a quiet period of solar activity, which enabled us to reliably associate the solar surface event with its counterpart observed in the Earth magnetosphere. In our study, we utilized (i) various tools to analyze a multi-wavelength data set that includes ground (BBSO vector magnetograms, Hα) and space (SOHO, TRACE, RHESSI and ACE) based data; (ii) linear force-free modeling to reconstruct the coronal field above the active region and (iii) erupting flux rope (EFR) model to simulate a near-Sun halo CME and a near-Earth interplanetary CME (ICME). Our findings indicate that persisting converging and shearing motions near the main neutral line could lead to the formation of twisted core fields and eventually their eruption via reconnection. In the discussed scenario, the *in situ* formed erupting loop can be observed as a magnetic cloud (MC) when it reaches the Earth. The EFR model was able to produce both a model halo CME and ICME providing a good global match to the overall timing and components of the magnetic field in the observed MC. The orientation of the model ICME and the sense of the twist, inferred from the EFR model, agree well with the orientation and the magnetic helicity found in the source active region.

1. Introduction

Shortly after coronal mass ejections (CME) were discovered (Tousey, 1973; Gosling *et al.*, 1974; MacQueen *et al.*, 1974), it was found that Earth directed ejecta are related to the occurrence of geomagnetic storms (Burlaga *et al.*, 1981; Wilson and Hildner, 1984). The primary cause of these intense storms are disturbances in the solar wind which are observed as long intervals of strong southwardly directed interplanetary magnetic field (IMF) supplied by CMEs (Rostoker and Fälthammar, 1967; Russell, McPherron, and Burton, 1974; Tsurutani *et al.*, 1992).

In this paper, we present detailed description and analysis of the May 13, 2005 eruption in NOAA AR 0759 and associated coronal and interplanetary phenomena.

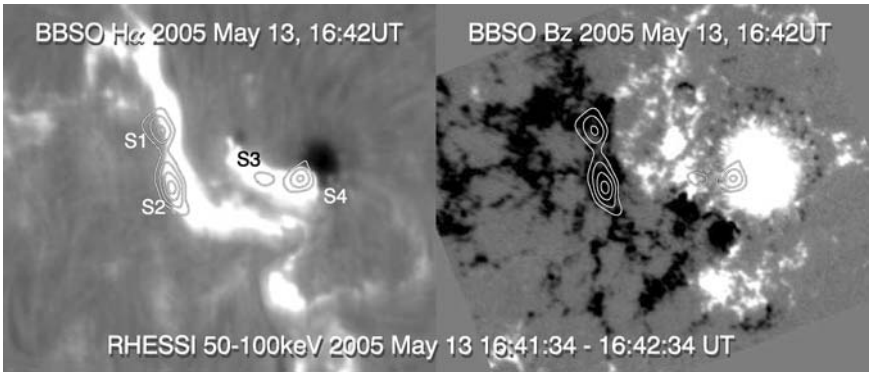

Figure 1. Partial frame of BBSO full-disk Hα image (*left*) and a line-of-sight magnetogram (*right*) taken at 16:42 UT. *Contours* show RHESSI hard X-ray emission in 50 – 100 keV energy band accumulated from 16:41:34 to 16:42:34 UT. Field of view is 230 × 195 arcsec. North is up, west is to the right.

Because the solar and heliospheric background conditions were relatively simple for this event, it was possible to unambiguously relate the solar surface event and the associated interplanetary disturbance that caused a strong geomagnetic storm (KYOTO provisional $\mathrm{Dst}_{\mathrm{min}}$ index $= -263$ nT). In our study, we utilized (i) a multi-wavelength data set that includes ground (BBSO vector magnetograms, Hα) and space (SOHO, TRACE, RHESSI and ACE) based data; (ii) linear force-free modeling to reconstruct the coronal fields above the active region and (iii) emerging flux rope model to simulate a near-Sun halo CME and near-Earth interplanetary CME as well as to compare the simulations to the overall timing of the event and to the various field components as observed by ACE satellite.

2. Solar Data and Analysis

The eruption that began at 16:03 UT on May 13, 2005 in AR NOAA 0759 was associated with a fast halo CME and an intense geomagnetic storm ($\mathrm{Dst}_{\mathrm{min}} = -263$ nT) that commenced on early May 15th. In Figure 1, we show BBSO Hα image of the flare and a line-of-sight magnetogram taken at 16:42 UT during the impulsive phase. Overplotted contours respresent RHESSI hard X-ray (HXR) sources detected in a broad 25 – 100 keV energy band. Time profiles of both Hα and RHESSI emission are shown in Figure 2. The images indicate that this was a typical two-ribbon flare that developed in a bi-polar magnetic configuration. The east ribbon was located in an area of negative magnetic fields (black), while the west ribbon was largely associated with the main sunspot of positive polarity. This sunspot displayed a spiral structure with left-handed twist, indicating negative helicity. According to Hα data, the extended north–south oriented FN filament seen in the upper part of Figure 3, *right* did activate about 30 minutes prior the eruption and it became darker and

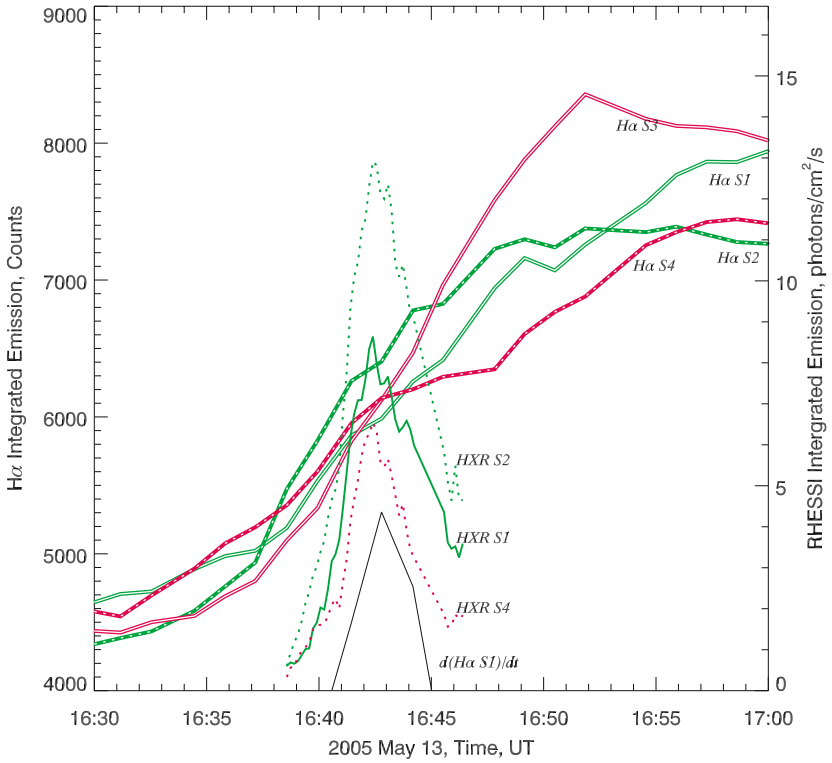

Figure 2. Light curves for the M8.0 May 13, 2005 flare. *Thick lines*, denoted with "Hα", represent Hα light curves (*left axis*) determined in the areas covered by RHESSI HXR sources S1 – S4 (see Figure 1). RHESSI light curves (*right axis*) are shown with *thin lines* denoted with "HXR". *Black solid line* is the time derivative of the light curve from Hα source S1. For display purposes the true values of the derivative were divided by 2.3.

bigger. With the onset of strong flare emission at 16:31 UT the filament mostly ceased to be observed in Hα spectral line, however, faint traces of it could be seen throughout the entire length of the flare (see also Figure 3 in Qiu and Yurchyshyn (2005)). This Hα filament restored its shape and appearance before the flare was over. As to the FS filament, it did not exhibit any significant signs of activation prior to the event, however after the flare peak it became obvious that the shape of the filament has changed: its southern extreme was now curved toward west, pointing to the main sunspot (see dashed line in Figure 3, *right* and compare panels a and c in Figure 3 in Qiu and Yurchyshyn (2005)).

2.1. TIME PROFILES OF Hα AND RHESSI FLARE EMISSION

The May 13 flare was associated with strong Hα emission from two flare ribbons (Figure 1, *left*) as well as four RHESSI hard X-ray (HXR) sources that could be

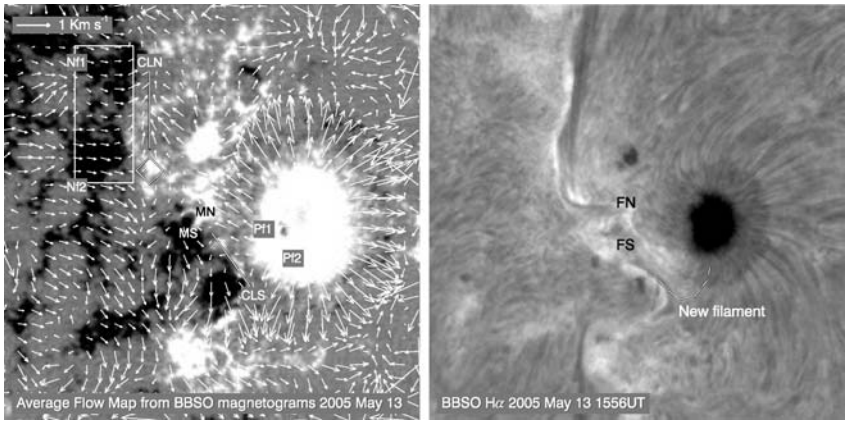

Figure 3. Left: Averaged flow map calculated from 107 BBSO line-of-sight magnetograms recored between 15:43 and 19:44 UT on May 13, 2005. The maximum velocity in the sunspot moat just north the main sunspot is approximately 1 km second^{-1}, r.m.s. = 300 m second^{-1}. The *rectangle* indicates the position of RHESSI HXR sources S1 and S2, CLN and CLS are lines of converging horizontal flows, the *diamond* marks the stagnation point in the flow pattern and MN and MS are the areas where the northern and southern filaments are rooted (see *right panel*). *Right*: BBSO Hα image taken at 15:56 UT prior the flare onset. The flare ribbons developed along the northern (FN) and southern (FS) filaments. The *dashed curve* indicates the new location of the FS filament (see text).

detected in a broad 25 – 100 keV energy band (noted in Figure 1 as S1, S2, S3 and S4). Contours in Figure 1 show RHESSI HXR emission integrated between 16:41:34 and 16:42:34 UT. S1 and S2 sources were located inside the eastern flare ribbon and relatively strong (−200 to −350 G) negative polarity fields, while S3 and S4 were within the positive polarity (300 – 450 G) penumbra of the main sunspot. This fact agrees very well with the trap/precipitation model by Melrose and White (1979), which predicted that flux asymmetry of hard X-ray footpoints in flaring loops could be caused by a magnetic asymmetry of a loop. In this model, stronger magnetic fields in one leg of a magnetic loop mirrors a fraction of precipitating electrons thus reducing HXR emission at this footpoint. A recent study by Schmahl, Pernak, and Hurford (2006) supported the prediction.

Figure 2 shows time profiles of Hα emission (HαS1 – S4, thick double lines) calculated over the areas covered by the RHESSI sources. The three overlaid curves that peak at 16:42:30 UT (thin lines) correspond to the HXR time profiles from S1, S2 and S4 sources. Emission from S3 was relatively weak and is not shown in this graph. Cleaned RHESSI images with a 10 seconds cadence (integrated over 60 seconds period) and 9.8″ FWHM resolution (using grids 3 – 9) were used to generate the image sequence and to derive the light curves of the HXR emission. The graph shows that the impulsive phase of the Hα flare started at about 16:31 UT and the time profiles from all four Hα areas are similar. The lower curve shows the time derivative, $d(H\alpha S1)/dt$, calculated from HαS1 light curve, which corresponds very well to the HXR time profiles implying that chromospheric plasma

heating and subsequent Hα emission was caused by fast electrons accelerated at the reconnection site (Neupert, 1968; Dennis and Zarro, 1993). We note, that in order to make this graph less busy we do not plot here time derivatives from the other 3 Hα sources, which are similar to that shown in Figure 2. The simple structure of the flare emission, similarity between all four Hα and RHESSI time profiles, as well as the fact that the time derivative of Hα emission coincides in time with the position of the HXR peaks, all indicate that this flare could be caused by reconnection between two independent magnetic flux systems, as opposed to reconnection between multiple flux systems suggested, *e.g.*, in the break-out model (Antiochos, 1998; Antiochos, DeVore, and Klimchuk, 1999). Examples of complex flare emission can be found in Yurchyshyn *et al*. (2004, 2006).

2.2. HORIZONTAL PLASMA FLOW

Figure 3 shows an average flow map calculated from BBSO line-of-sight magnetograms that cover an extended period of time (15:43 – 19:44 UT). This period includes both pre- and post-flare evolution. The final map was generated by averaging 106 individual flow maps produced by local correlation tracking technique (November and Simon, 1988) with the FWHM of the tracking window of 6×6 arcsec and a 1 minute correlation interval. This averaged flow map therefore represents large-scale and persisting plasma flows.

The white rectangle in the figure marks the location of RHESSI HXR sources S1 and S2 that were associated with negative polarity magnetic fields Nf1 and Nf2. Pf1 and Pf2 indicate the location of S3 and S4 sources and refer to the positive magnetic polarity associated with them. The two dark filaments FN and FS, seen in the pre-flare Hα image (Figure 3), had one of their footpoints anchored in the vicinity of MN and MS magnetic concentrations (Figure 3, *left* panel). These polarities are connected by a system of dark arches, which indicates that MN and MS most probably composed one magnetic dipole. This dipole was observed on the day prior to the flare and therefore cannot be considered as a rapidly emerging flux.

The most intense horizontal flows were observed in the moat that surrounds the sunspot penumbra. The moat outflow reached speeds of about 1 km s^{-1}, while elsewhere the intensity of the flow varied in the range of 100 – 300 m second^{-1}. The flow pattern in the vicinity of the major neutral line (NL) has two components: converging and shearing flows. Segments of double black lines in Figure 3 indicate two convergence lines, CLN and CLS, where oppositely directed flows, associated with the negative polarity fields and the main sunspot, merge. The converging flows at the CLS line are not as evident as at the CLN line due to insufficient spatial resolution of the flow map and complex pattern of small-scale motions. The radial moat outflow from the main sunspot in the SE direction stops at the negative field concentration, which was moving perpendicular (in the SW direction) to this radial outflow. Although this flow interaction does not exhibit the classical converging

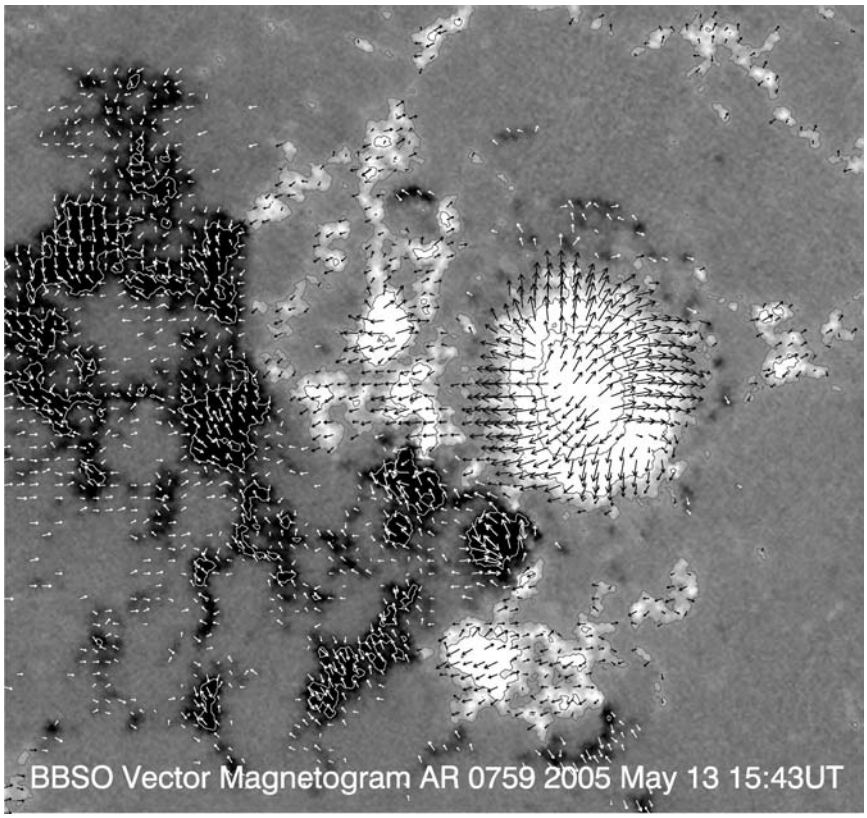

Figure 4. 15:43 UT BBSO vector magnetogram resolved for 180° ambiguity.

pattern it, nevertheless, promotes magnetic field cancellation and magnetic stress build up. The converging lines are separated by a stagnation point in the flow pattern (diamond) and a dipole MN–MS. CLN line is slightly displaced from the main NL and has a shear component directed northward, while CLS has a southward component. The converging and shearing motions that are seen at two different converging lines may be indicative that two independent systems of helical magnetic fields could form above the CLN and CLS neutral lines due to the cancellation process as suggested by van Ballegooijen and Martens (1989) and further explored by Linker *et al*. (2005) and Welsch (2006).

2.3. VECTOR MAGNETOGRAMS AND ELECTRIC CURRENTS

BBSO Digital Vector Magnetograph (DMG) fully covered the event and produced a set of 1 minute cadence vector magnetograms with 0.6 arcsec pixel size. Figure 4 shows an example of DMG data taken before the flare onset at 15:43 UT. In general, the active region had a relatively simple magnetic configuration with smooth

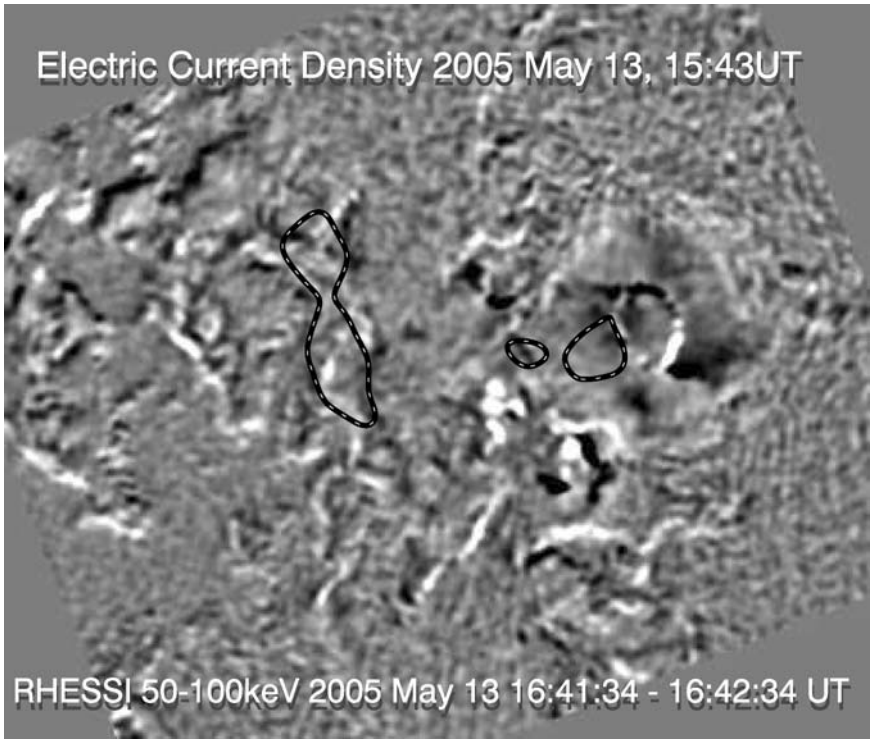

Figure 5. Distribution of electric current density calculated from the 15:43 UT vector magnetogram. *Black/white* corresponds to ±9000 A m^2. Positive (*white*) currents are upward. *Contour lines* show RHESSI hard X-ray emission in the 50 – 100 keV energy band accumulated from 16:41:34 to 16:42:34 UT. Field of view is 230 × 195 arcsec. Solar north is up, east is to the left.

variations of the transverse field. The main spot was uniformly twisted counter clockwise (negative helicity). Due to insufficient sensitivity of the instrument, magnetic field measurements within the sunspot umbra are not reliable. The 180° ambiguity was resolved by applying a potential field method (Abramenko, 1986). Recent study in the framework of SDO/HMI – CSAC Azimuth Ambiguity Resolution Workshop (Metcalf *et al*., 2006) showed that this method can correctly resolve ambiguity for about 90% of strong transverse magnetic fields, which makes it quite applicable in cases of simple magnetic configurations.

Vector magnetogram data were used to calculate density distribution of vertical electric currents in the active region. Thus, Figure 5 shows that highest current density was associated with two small negative polarity magnetic concentrations just SE of the main sunspot. This area was also the location of strong converging flows at the CLS line (Figure 3). Note that the "O"-shaped structure in the center of the sunspot is an artifact caused by the insufficient counts inside the very dark umbra. Contours, plotted over the current density map, show the location of RHESSI HXR emission and it appears that these HXR sources were not co-located with strong

electric current densities, which agrees with earlier reports (de La Beaujardiere, Canfield, and Leka, 1993; Leka *et al*., 1993).

Earlier, Abramenko, Gopasiuk, and Ogir (1991, 1993) reported that the intensity and the lifetime of Hα and HXR flare emission, associated with upward currents, were fount to be higher than those associated with downward currents. Authors suggested that upward currents could contribute to the acceleration of electrons traveling downward to the photosphere and thus enhance flare emission in those places. In this context, we calculated the net current over the area covered by HXR sources S1, S2, S3 and S4. Thus, electric current imbalance inside the combined area S1 + S2 was about 20% and the upwardly directed net current was about 2.5×10^{11}A. The current imbalance in the area S3 + S4 was -4% and the downward net current was about -4.3×10^4 A. Note, that S1 and S2 sources were the most intense (see Figure 2) and that the net current associated with them was upward. These results, therefore, support the earlier idea that strong upward electric currents could supply additional energy to the downward moving electrons thus contributing to the asymmetry of the X-ray flare emission at the footpoints of the flare loops.

2.4. Structure of magnetic fields

Figure 6 shows coronal magnetic fields above the active region as seen in the pre-flare TRACE 171Å image taken at 12:58 UT. Here, positive and negative magnetic fields associated with RHESSI HXR sources S1 – S4 are marked by Pf1, Pf2, Nf1, Nf2. Three main features can be distinguished in this image (see also the inset): (i) rising, bright, reverse "S" shaped fields, indicated by the black and white dotted curve and located above the dark FN Hα filament (Figure 3); (ii) two bright loop systems rooted at Pf1–Nf1 and Pf2–Nf2 and (iii) two low density voids encompassed by the loop systems Pf1–Nf1 and Pf2–Nf2. We thus speculate that these structures in the TRACE 171Å image are indicative of a flux rope(s) present in the active region.

We used a linear force-free method (Abramenko and Yurchyshyn, 1996) to model the coronal field above the active region. A 16:03 UT full-disk MDI magnetogram (Figure 7, *background*) was used as a photospheric boundary condition and we further assumed that the magnetic field was in the potential state everywhere on non-photospheric boundaries of a 3D volume. The numerical solution was obtained for a volume of size $156 \times 204 \times 243$ arcsec with the size of a grid cell of $1.98 \times 1.98 \times 2.79$ arcsec. The best fit between the field-line features in the TRACE image and the model field lines was obtained with the parameter $\alpha = -0.025$ arcsec^{-1}.

In Figure 7, we show modeled force lines that originate within the SE part of the sunspot (locations of HXR sources S3 and S4 and the west flare ribbon) and divided into two groups depending on where these field lines end. Thus, the model indicates that source S4 could be located in a region which was common to the footpoints for two otherwise-independent magnetic flux systems, while their other

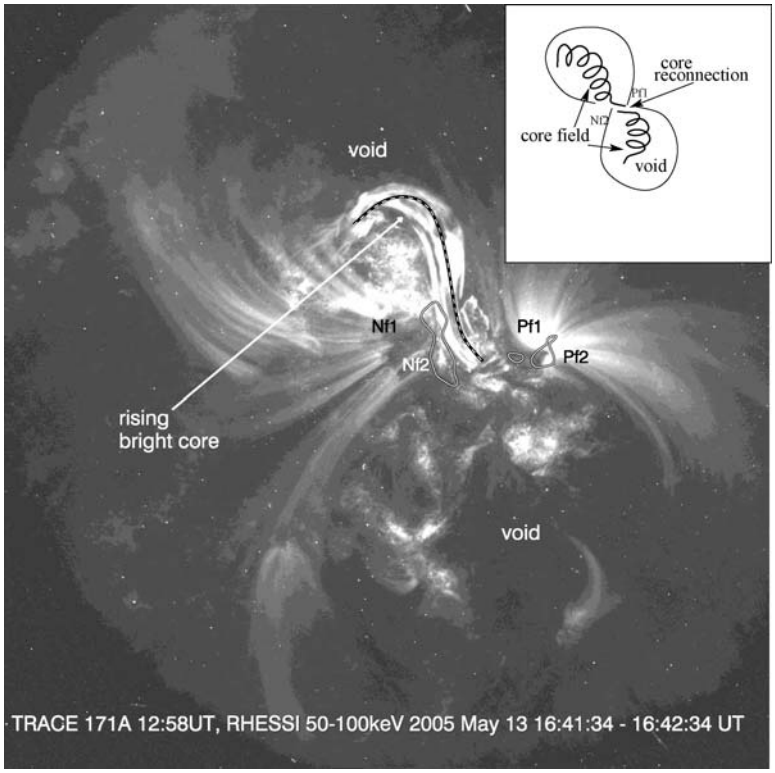

Figure 6. 12:58 UT TRACE 171 Å image. *Contours* show RHESSI hard X-ray emission in 50 – 100 keV energy band accumulated from 16:41:34 to 16:42:34 UT. The *black and white curve* traces the reverse "S" shaped rising bright core. *Inset* shows that this magnetic configuration could contain flux ropes suspended above neutral lines and surrounded by large-scale coronal fields. Please note that the number of turns in the core fields is exaggerated.

footpoints were separated and associated with S1 and S2 sources. This inference is supported by Figure 6, which shows that the two different TRACE loop systems, described above, are rooted at Pf1 and Pf2 and share one common RHESSI source S4 (contour), while their other footpoints, anchored at Nf1 and Nf2, were associated with S1 and S2.

We further speculate that converging and shearing flows could, according to the cancellation model (van Ballegooijen and Martens, 1989), lead to formation of these two systems of independent magnetic loops and to the build up of free magnetic energy in the coronal field (Welsch, 2006). As the flux strengthens due to continuous inflows, it may slowly expand and rise above the photosphere due to loss of stability and transition to a neighboring state of equilibrium. Note that the time scale of flux injection into a flux rope via cancellation process is rather large and thus allows the magnetic configuration to "absorb" the new flux without catastrophic eruptions. Thus, the pre-flare TRACE image shows that the bright

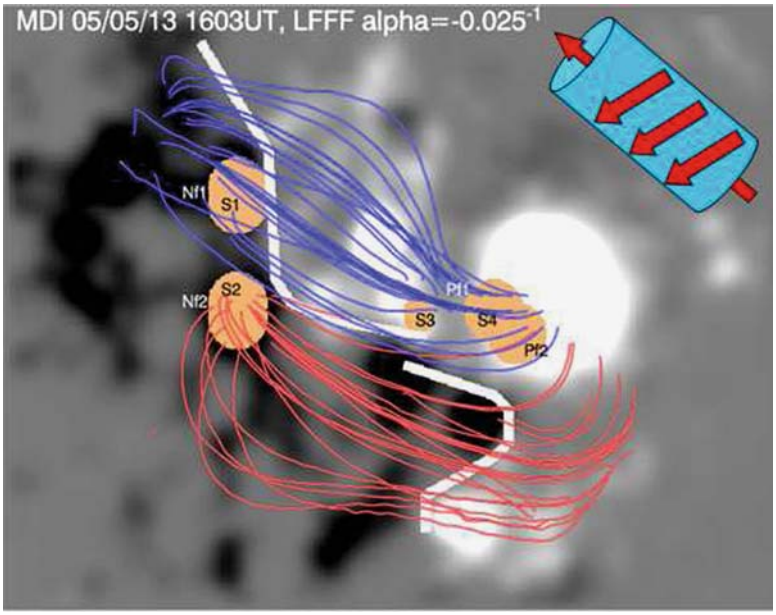

Figure 7. Background: A partial frame of an MDI full-disk magnetogram of AR NOAA 0759 recorded at 16:03 UT. Over-plotted *force lines* are calculated from a linear force-free model with parameter $\alpha = -0.025$ arcsec^{-1}. *Filled areas* mark the location of RHESSI HXR sources S1 – S4 (see also Figure 1). Two *thick white lines* indicate the location of Hα filaments FN and FS. The *blue cylinder* in the *upper right corner* shows directions of the axial and azimuthal fields in a model MC derived from the erupting flux rope model (see Section 3.2).

dense core, which is seen suspended above the neutral line in the 12:58 UT TRACE 171 Å frame became active and started its slow ascent as early as 12:00 UT. The persistent converging flows could drive the magnetic configuration to a critical state when gradual changes at the photospheric magnetic boundary could no longer be accommodated by quasi-steady evolution of coronal fields.

Therefore we suggest that the May 13 eruption proceeded according to the tether-cutting model (Moore and LaBonte, 1980) where the eruption between the two independent sheared flux systems was initiated due to reconnection process in the core field, which gradually involved large-scale fields enveloping the core field. The four RHESSI HXR sources could then be caused by magnetic reconnection between two sheared loop systems Pf1–Nf1 and Pf2–Nf2 that occurred high in the corona.

The outcome of this reconnection process will be one large-scale magnetic system that would directly connect the leading and following part of the active region. In the discussed scenario, erupted magnetic fields should be co-aligned with the large-scale structure of the active region, *i.e.* the footpoints of the erupted loop (CME) are rooted in the leading positive and following negative fields. The

orientation of the CME is then expected to follow the orientation of the major NL that runs approximately along the SW–NE line and its predominant twist should be the same as that of the active region (negative helicity). This suggestion can be tested by analyzing interplanetary magnetic field data obtained from the ACE spacecraft.

3. Interplanetary Manifestation

3.1. ERUPTING FLUX ROPE MODEL

Krall *et al*. (2006) showed that the erupting flux rope (EFR) model (Chen and Garren, 1993; Chen, 1996; Krall, Chen, and Santoro, 2000) was able to reproduce many details of the CME/ICME event on October 28 – 30, 2003. These results present another evidence of a strong correlation between the magnetic field in an active region and that in the corresponding ICME (Bothmer and Schwenn, 1994; Rust, 1994; Marubashi, 1997; Zhao and Hoeksema, 1998; Crooker, 2000; McAllister and Martin, 2000; Yurchyshyn *et al*., 2001; Nindos, Zhang, and Zhang, 2003; Ruzmaikin, Martin, and Hu, 2003; Hu *et al*., 2005; Luoni *et al*., 2005; Mandrini *et al*., 2005; Rust *et al*., 2005; Yurchyshyn, Hu, and Abramenko, 2005). Here, we further investigate the relationship between solar magnetic fields in the May 13, 2005 event and the associated ICME at 1 AU. In modeling the May 15, 2005 ICME event, we endeavor to reproduce the near-Sun CME morphology and dynamics, as observed in LASCO coronagraph.

The erupting flux rope model (Chen and Garren, 1993; Chen, 1996; Krall, Chen, and Santoro, 2000) follows the motion of the apex of a three-dimensional flux rope that has footpoints rooted below the photosphere. In the model calculation, all flux rope plasma and field quantities are functions of the distance from the Sun, Z, and flux rope minor radius, a (see Figure 2 in Krall *et al*., 2001) and are evaluated at each time step. The version of the code that was used in this study is that of the Krall *et al*. (2006) with the elliptical flux rope shape instead of the circular shape (the appendix in Krall *et al*. (2006) paper describes the model updates).

We would like to emphasize that because the model focuses on the dynamics of a pre-existing solar flux rope, the process of flux-rope formation is not addressed. Moreover, in this study the EFR model is exclusively used as a magnetic cloud fitting tool without discussing the model driver mechanism and the propagation of the flux rope in interplanetary media.

The driving forces that generate the outward motion of the flux rope are: $J \times B$ hoop force, the pressure force, the inward-directed "tension" due to the toroidal field, gravity forces, drag, and the radial $J_t \times B_C$ force, where J_t is the component of the current flowing parallel to the flux rope axis and B_C is the component of the background coronal field that is perpendicular to both the flux rope axis and its direction of motion. That is, B_C represents overlying field that the flux rope

must push aside as it expands outwards. In this model, the drag term accounts for specific physical processes such as momentum coupling between the flux rope and the solar wind through which it passes and the resulting MHD wave and shock generation.

The model flux rope is initially in an equilibrium state and is driven to eruption by an increase in the helicity via a specified increase in the poloidal flux versus time. The interpretation of this helicity increase, which could result from either macroscopic reconnection or from a process that drives a current along the length of the flux rope, has been discussed elsewhere (Krall *et al*., 2001; Chen and Krall, 2003).

In order to obtain the best fit between the arrival time and the magnetic field intensity given by the model and the observed data at 1 AU we vary only four parameters: the amount of poloidal magnetic flux "injected" over a time of 1 h (final value of 4.4×10^{22} Mx), the intensity of the overlying field near the initial flux rope apex position that stabilizes the flux rope (6 G), the interplanetary drag coefficient (1.15), the eccentricity of the flux rope ellipse (0.87), and the initial density of the cold plasma in the prominence (2.1×10^8 cm^{-3}). The interplanetary solar wind speed in the model was set at 450 km second^{-1} to match the pre-event speed at 1 AU. Other parameters, such as initial flux-rope geometry (height and foot point separation) were set to typical values (Krall *et al*., 2006). The geometry affects the very-near-Sun flux-rope acceleration profile, which is not observed in this case. Subsequent dynamics are not sensitive to these parameters.

Once these parameters are set at the beginning of a run they (or any other parameters) they remain constant during calculations. Each run produces a flux rope that is then oriented in space in such a way that the model generated magnetic field profiles match the profiles observed with a satellite. Below, we describe this process in more details.

3.2. MAY 13, 2005 CME/ICME EVENT

The May 13, 2005 CME first appeared in the LASCO/C2 coronagraph field of view at 17:22 UT. The only full frame LASCO C3 image (17:42 UT, Figure 8, *left*) taken during the ejecta shows the CME seen as a "halo" around the occulting disk. According to the CME Catalog, this halo CME was rapidly expanding with the plane of sky speed exceeding 1650 km second^{-1}. The ejecta reached the Earth on May 15, 2005 and caused an intense geomagnetic storm. Figure 9 shows the corresponding solar wind data (solid curves) as measured at 1 AU by the SWEPAM (McComas *et al*., 1998) and MAG (Smith *et al*., 1998) instruments on board ACE. The associated ICME was a cloud-like structure (its boundaries indicated by vertical lines) with a smoothly rotating B_z component and a relatively low density. The MC arrived at about 06:00 UT (day of year 135.25) and it ended at about 19:12 UT (day

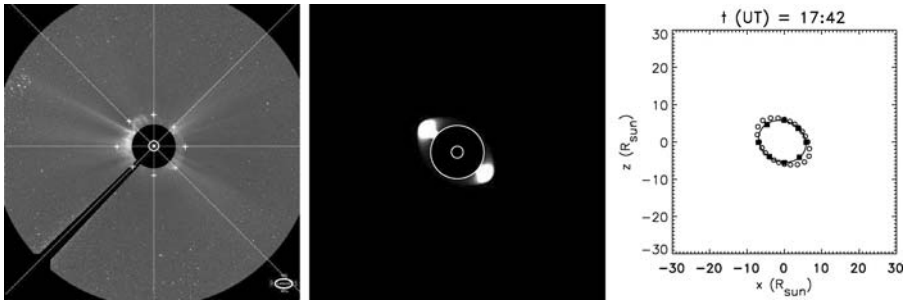

Figure 8. Left: LASCO/C3 17:42 UT image of the halo CME on May 13, 2005. Eight points ("+"), evenly spaced in position angle (*straight lines*), were measured along the outer edge of the halo. CME properties such as the size, shape and orientation can be quantified by fitting a model halo CME to the measured points. *Middle*: A synthetic coronagraph image of the model halo CME. The bright patches on both sides of the occulting disk in this image indicate the legs of the flux rope, which are typically more pronounced in the model than in the data. *Right*: Model-data comparison corresponding to the 17:42 UT LASCO C3 image. Here, the orientation angles are set at fixed values, chosen to provide a "best-fit" to the observed coronagraph image for this event. *Open circles* show the outline of the model flux rope and *dark boxes* are measurements from the LASCO C3 image (*left*).

of year 135.8). This ICME featured a velocity of about 900 km second^{-1} and an interplanetary (IP) shock at its leading edge. This ACE event showed a well-defined counter streaming electron flow between 05:30 UT on May 15 and at least 08:00 UT on May 18 (Gosling, 2006), which indicates that the flux rope remained connected to the solar photosphere, when it was detected at 1 AU.

For the purpose of orienting the 3D flux-rope geometry, we define a coordinate system with its origin at Sun center, the z-axis northward, the x-axis directed towards the west limb and the y-axis directed along the Earth–Sun line, away from Earth. When orienting the model flux rope, we include five angles: source latitude, λ_0, (for the May 13, 2005 event $\lambda_0 = 12$N), source longitude ($\phi_0 = 11$E), a tilt in the direction of latitude (α_x), a tilt about the direction of motion of the flux rope apex (α_y, *i.e.*, the orientation of the large axis of the ellipse measured clockwise (CW) from the x direction (west), and a tilt in the direction of longitude (α_z).

To quantify the observed CME morphology, eight points, evenly spaced in position angle, were measured along the outer edge of the ejecta (Figure 8, *left*). At each angle, the edge of the halo is chosen to be the outermost point on the overall expanding CME structure. In order to visualize the shape, size and orientation of the model halo CME, the 3D flux-rope geometry is constructed by computing the positions of a large number of points, which outline the flux rope's exterior surface; to obtain synthetic coronagraph images, interior points and density values must also be computed. In this model-data comparison, the orientation angles are set at fixed values, chosen to provide a best global fit to the only coronagraph image available for this event. Specifically, after each "run" of the model, the orientation angles were

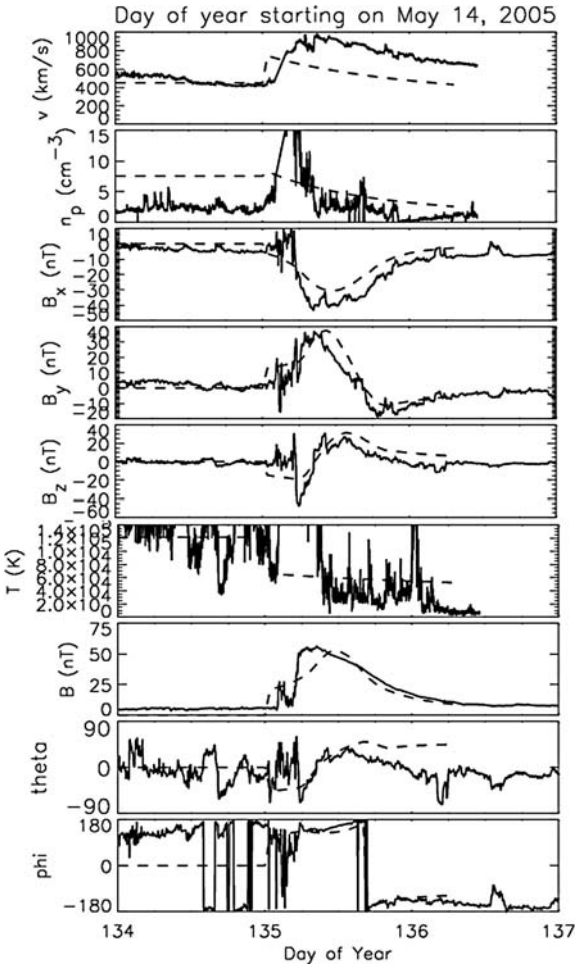

Figure 9. Data-model comparison for the May 15, 2005 ICME. *Solid lines* represent ACE measurements in the GSE coordinate system of various parameters of the May 15, 2005 MC taken at 1 AU (from top to bottom): solar wind speed, density, B_x, B_y and B_z components of the magnetic field, temperature, the magnitude of the magnetic field and the cone, *theta*, and clock, *phi*, orientation angles of the magnetic field vector. *Dashed lines* are the corresponding *in situ* curves generated from the EFR model.

adjusted, by trial and error, to obtain the best fit, on average, to the measured halo points while maintaining agreement with the Sun–Earth ICME transit time and the flux-rope field amplitude at 1 AU. Note that the computed flux-rope dynamics are independent of the orientation angles: that is the orientation angles can be adjusted without re-computing the model.

The inferred position of the flux rope for the May 13, 2005 event is shown in Figure 8, where the outline of the projected model-CME halo is indicated by the open dots, while the solid boxes correspond to positions measured in the

coronagraph image. We note that the elongation of the halo in the best-fit model solution, which is somewhat more pronounced than the elongation of the actual halo, indicates the direction of the flux-rope axis. This can be seen in the synthetic coronagraph image in Figure 8, which shows a top view of an expanding loop. The bright patches on both sides of the occulting disk in this image indicate the legs of the flux rope, which are typically more pronounced in the model than in the data. We shall see that our choice of near-Sun orientation angles is close to the correct orientation for the model ICME fields at 1 AU.

For the EFR model, model-data comparisons in the near-Earth region can be accomplished by evolving the model flux rope beyond the L1 point at 1 AU and by applying the orientation angles as in the near-Sun comparison. Equivalent *in situ* curves were then generated by diagnosing the position of Earth within the model flux rope and determining model field, density, velocity, *etc*., at that point. In order to obtain the directions of ICME field, the handedness of the flux rope and the sign of the leading-edge field must be specified (model dynamical results are independent of these two quantities). These selections were guided by ACE measurements which show that in the May 15, 2005 MC the leading-edge field was negative turning into positive, while the B_y component was positive. This indicates a left-handed MC.

In order to obtain model-data match at 1 AU, we had to change the orientation angles α_x, α_y and α_z, while source location angles (λ_0 and ϕ_0) and all other model inputs have been held constant. The orientation angle, α_y, was increased from 215 to 220°, corresponding to a 5° CW rotation of the halo away from the ecliptic plane. The tilt angle, α_z, was decreased from 11 to 8°, corresponding to a 3° deflection towards the solar disc center, relative to the Earth–Sun line, while α_x was increased by about 3° which correspond to deflection of the flux rope toward south pole. In practice, EFR input parameters are adjusted to obtain an optimum match to both the SOHO and ACE data, with *only* α_x, α_y, and α_z being allowed to vary between the near-Sun and near-Earth solutions.

Figure 9 shows a model-data comparison at 1 AU for the event. The model results (dashed curves) provide a good match to the overall transit time and various field components as observed by ACE satellite (solid curves), however, typical model velocities are lower by 35% relative to concurrent ACE velocities. Because the interplanetary dynamics are so ill-understood at present, it is possible that the actual interplanetary forces, such as solar wind drag, differ greatly enough from the model to routinely produce a higher velocity (relative to the model), with the same transit time. Because the near-Sun velocity is not well-constrained in this event, both (model and observed) velocities, therefore, may be mismatched, while the average transit velocities and the transit times are correct. More distant possibility that may contribute is that the CME path may be curved along the Parker spiral, while the model assumes a straight path directly from the Sun to the Earth. The shorter path of the model CME allows the same transit time with a smaller velocity.

3.3. Comparison between the magnetic fields in the active region and in the ICME

(1) In Section 2.4, we found that the coronal magnetic field above the active region can be very well approximated by a linear force-free model with $\alpha = -0.025$ arcsec^{-1} implying that negative twist dominated this magnetic region. The same sense of twist was found in the MC, associated with the eruption, by fitting of the observed data with the EFR model.

(2) The average angle between the direction of the force-free lines (they are directed from north (white) to south (black) polarity in Figure 7) and the solar west is about 210°. This compares well with the orientation angles of the model CME ($\alpha_y = 215°$ near the Sun) and ICME ($\alpha_y = 220°$ near the Earth) as derived from the EFR model. Note that α_y is the angle measured clockwise from the x-axis (west, see Section 3.2) to the direction of the axial field in the MC.

(3) As determined from the EFR model, the toroidal (axial) flux, $F_t^{\rm EFR}$, confined in the model ICME was found to be about 2.9×10^{21} Mx, while the corresponding poloidal flux, $F_p^{\rm EFR}$, was about 4.4×10^{22} Mx. Note that the poloidal flux is the measure of magnetic twist in a flux rope. The model toroidal flux $F_t^{\rm EFR}$ is two times lower than the reconnection flux, $F_r = 6.2 \times 10^{21}$ Mx, reported for this event in Qiu and Yurchyshyn (2005). The reconnection flux was derived as integration of the line-of-sight magnetic field swept by the separating Hα flare ribbons (see Qiu *et al.*, 2004 for more details). Hu (2006) has calculated the toroidal (axial) and poloidal (twist) fluxes from a Grad-Shafranov reconstruction technique (Hu and Sonnerup, 2002) applied to the May 15 ACE event. For the axial flux, Hu finds 2.1×10^{21} Mx, which compares well to the EFR result (2.9×10^{21} Mx). For the poloidal flux, Hu reports 4.2×10^{21} Mx. Computation of the total poloidal flux, however, depends on global flux-rope geometry, which significantly differs in EFR and Grad-Shafranov technique, and therefore the numbers for the poloidal flux cannot be directly compared.

4. Conclusions and Summary

In this study, we present ground and space based data on the May 13, 2005 solar eruption, CME and the corresponding interplanetary ejecta observed near the Earth on May 15, 2005. This isolated two-ribbon M8.0 flare and the very fast CME occurred in a relatively simple magnetic configuration during a quiet period of solar activity. This enabled us to reliably associate the solar surface event with its counterpart observed in the Earth magnetosphere. Based on the analysis of an extended data set (solar ground and space based data as well as magnetospheric measurements at 1 AU) and results from numerical modeling, we concluded the following.

(1) A magnetic configuration in the active region was relatively simple and could be reasonably well approximated with a linear force-free model with negative parameter α indicating that negative magnetic helicity (left-handed twist) dominated in this active region.
(2) The flow pattern in the vicinity of the convergence lines CLN and CLS, as determined from a series of line-of-sight magnetograms, had two components: converging and shearing flows. These motions may be indicative that strong helical magnetic fields could form above the major neutral lines due to the cancellation process as suggested by van Ballegooijen and Martens (1989) and further explored by Linker *et al*. (2005) and Welsch (2006).
(3) RHESSI HXR sources observed in this event did not spatially coincide with strongest electric current concentrations, which agrees with earlier reports (de La Beaujardiere, Canfield, and Leka, 1993; Leka *et al*., 1993). However, the most intense HXR sources S1 and S2 were associated with strong magnetic fields (300 – 400 G) and upward net electric current of about 2.5×10^{11} A, while less intense S3 and S4 sources were located in the area of a weaker field (200 – 350 G) and downwardly directed net current of -4.3×10^4 A. This is in accord with earlier suggestions that asymmetry of magnetic configuration and upward electric currents could cause asymmetry of the X-ray emission at the footpoints of flare loops (Melrose and White, 1979; Abramenko, Gopasiuk, and Ogir, 1991, 1993; Schmahl, Pernak, and Hurford, 2006).
(4) The simple structure of flare emission, similarity between all Hα and RHESSI time profiles as well as the fact that the time derivative of Hα emission coincides in time with the position of the HXR peaks, suggest that the May 13, 2005 flare could be caused by reconnection between two independent magnetic flux systems.
(5) Erupting Flux Rope model was able to produce a model halo CME and an ICME that provided a good match to the overall timing and to the various field components of the MC observed by ACE spacecraft. The orientation of the model ICME (215°) and the sense of the twist (left-handed), inferred from the EFR model, agree well with the orientation (210°) and the magnetic helicity (negative) found in the active region that spawn this event. We would like to emphasize that in this event, as well as in the October 28, 2003 event (Krall *et al*., 2006), the direction in which the observed halo CME is elongated corresponds to the projected orientation of the MC, determined from the EFR model.

Finally, we speculate that persisting converging and shearing motions in the vicinity of the main magnetic neutral line could lead to a formation of strongly sheared and twisted core fields and eventually their eruption as according to the reconnection model (Moore and LaBonte, 1980). The product of this reconnection will be one large-scale magnetic loop that would directly connect the leading and following part of the active region. In the discussed scenario, this newly formed erupting loop can be observed as a magnetic cloud when it reaches the Earth. Since

this loop is connected to the Sun, we can reasonably expect that the orientation of the CME is more or less preserved as it propagates through interplanetary medium.

Acknowledgements

We thank anonymous referee for valuable suggestions and constructive criticism which improved the clarity of the paper. We are obliged to BBSO staff for their effort in obtaining the data. We thank the ACE MAG instrument team and the ACE Science Center for providing the ACE data. SOHO is a project of international cooperation between ESA and NASA. VY's work was supported under NSF grants ATM 0536921 and NASA grant NNG0-4GJ51G. CL's work was supported by NSF SHINE ATM-0548952 grant. VA acknowledges support under grant NNG0-5GN34G. JK's work was supported by NASA (DPR W-10106, LWS TRT program) and the Office of Naval Research.

References

Abramenko, V.I.: 1986, *Soln. Dannye, Bull. Glav. Astron. Obs.* **8**, 83.
Abramenko, V.I. and Yurchyshyn, V.B.: 1996, *Solar Phys.* **168**, 47.
Abramenko, V.I., Gopasiuk, S.I., and Ogir', M.B.: 1991, *Solar Phys.* **134**, 287.
Abramenko, V.I., Gopasiuk, S.I., and Ogir', M.B.: 1993, *Bull. Crimean Astrophys. Obs.* **87**, 1.
Antiochos, S.K.: 1998, *Astrophys. J.* **502**, L181.
Antiochos, S.K., DeVore, C.K., and Klimchuk, J.A.: 1999, *Astrophys. J.* **510**, 485.
Bothmer, V. and Schwenn, R.: 1994, *Space Sci. Rev.* **70**, 215.
Burlaga, L.F., Sittler, E., Mariani, F., and Schwenn, R.: 1981, *J. Geophys. Res.* **86**, 6673.
Chen, J.: 1996, *J. Geophys. Res*. **101**, 27499.
Chen, J. and Garren, D.A.: 1993, *Geophys. Res. Lett*. **20**, 2319.
Chen, J. and Krall, J.: 2003, *J. Geophys. Res.* **108**, SSH 2-1, CiteID 1410, DOI: 10.1029/2003JA009849.
Crooker, N.U.: 2000, *J. Atmos. Sol.-Terr. Phys*. **62**, 1071.
de La Beaujardiere, J.-F., Canfield, R.C., and Leka, K.D.: 1993, *Astrophys. J*. **411**, 378.
Dennis, B.R. and Zarro, D.M.: 1993, *Solar Phys*. **146**, 177.
Gosling, J.T.: 2006, *private communication.*
Gosling, J.T., Hildner, E., MacQueen, R.M., Munro, R.H., Poland, A.I., and Ross, C.L.: 1974, *Astrophys. J*. **79**, 4581.
Hu, Q.: 2006, *private communication*.
Hu, Q. and Sonnerup, B.U.: 2002, *J. Geophys. Res*. **107**, CiteID 1142, DOI: 10.1029/2001JA000293.
Hu, Q., Smith, C.W., Ness, N.F., and Skoug, R.M.: 2005, *J. Geophys. Res*. **110**, A09S03, DOI: 10.1029/2004JA010886.
Krall, J., Chen, J., and Santoro, R.: 2000, *Astrophys. J*. **539**, 964.
Krall, J., Chen, J., Duffin, R.T., Howard, R.A., and Thompson, B.J.: 2001, *Astrophys. J*. **562**, 1045.
Krall, J., Yurchyshyn, V.B., Slinker, S., Skoug, R.M., and Chen, J.: 2006, *Astrophys. J*. **642**, 541.
Leka, K.D., Canfield, R.C., McClymont, A.N., de La Beaujardiere, J.-F., Fan, Y., and Tang, F.: 1993, *Astrophys. J*. **411**, 370.
Linker, J.A., Mikic, Z., Titov, V., Lionello, R., and Riley, P.: 2005, *AGU Spring Meeting 2005*. Abstract **#SH54B-05**.

Luoni, M.L., Mandrini, C.H., Dasso, S., van Driel-Gesztelyi, L., and Démoulin, P.: 2005, *J. Atmos. Sol.-Terr. Phys.* **67**, 1734.
MacQueen, R.M., Eddy, J.A., Gosling, J.T., Hildner, E., Munro, R.H., Newkirk, G.A., Jr., Poland, A.I., and Ross, C.I.: 1974, *Astrophys. J.* **187**, L85.
Mandrini, C.H., Pohjolainen, S., Dasso, S., Green, L.M., Démoulin, P., van Driel-Gesztelyi, L., Copperwheat, C., and Foley, C.: 2005, *Astron. Astrophys.* **434**, 725.
Marubashi, K.: 1997, in N. Crooker, J.A. Joselyn, and J. Feynman (eds.), *Coronal Mass Ejections*, Geophysical Monograph 99, AGU, Washington, DC, p. 147.
McAllister, H. and Martin, S.F.: 2000, *Adv. Space Res.* **26**, 469.
McComas, D.J., Bame, S.J., Barker, P., Feldman, W.C., Phillips, J.L., Riley, P., and Griffee, J.W.: 1998, *Space Sci. Rev.* **86**, 563.
Melrose, D.B. and White, S.M.: 1979, *Proc. Astron. Soc. Aust.* **3**, 369.
Metcalf, T.R., Leka, K.D., Barnes, G., Lites, B.W., Georgoulis, M.K., Pevtsov, A.A., Gary, G.A., Jing, J., Balasubramaniam, K.S., Li, J., Liu, Y., Wang, H.N., Abramenko, V., Yurchyshyn, V., and Moon, Y.-J.: 2006, *Solar Phys.* **237**, 267.
Moore, R.L. and LaBonte, B.: 1980, in M. Dryer and E. Tandberg-Hanssen (eds.), *IAU Symp.* 91, Solar and Interplanetary Dynamics, Reidel, Boston, p. 207.
Nindos, A., Zhang, J., and Zhang, H.: 2003, *Astrophys. J.* **594**, 1033.
Neupert, W.M.: 1968, *Astrophys. J.* **153**, L59.
November, L.J. and Simon, G.W.: 1988, *Astrophys. J.* **333**, 427.
Qiu, J. and Yurchyshyn, V.: 2005, *Astrophys. J.* **634**, L121.
Qiu, J., Wang, H., Cheng, C.Z., and Gary, D.E.: 2004, *Astrophys. J.* **604**, 900.
Rostoker, G. and Fälthammar, C.-G.: 1967, *J. Geophys. Res.* **72**, 5853.
Russell, C.T., McPherron, R.L., and Burton, R.K.: 1974, *J. Geophys. Res.* **79**, 1105.
Rust, D.M.: 1994, *Geophys. Res. Lett.* **21**, 241.
Rust, D.M., Anderson, B.J., Andrews, M.D., Acuña, M.H., Russell, C.T., Schuck, P.W., and Mulligan, T.: 2005, *Astrophys. J.* **621**, 524.
Ruzmaikin, A., Martin, S.F., and Hu, Q.: 2003, *J. Geophys. Res.* **108**, 1096, DOI: 10.1029/2002 JA009588.
Schmahl, E.J., Pernak, R., and Hurford, G.: 2006, *American Astronomical Society, SPD Meeting 37*. Abstract **#13.08**.
Smith, C.W., Acuña, M.H., Burlaga, L.F., L'Heureux, J., Ness, N.F., and Scheifele, J.: 1998, *Space Sci. Rev.* **86**, 613.
Tousey, R.: 1973, in M.J. Rycroft and S.K. Runcorn (eds.), *COSPAR Space Research XIII*, Akademie Verlag, Berlin and Pergamon, Oxford, p. 713.
Tsurutani, B.T., Lee, Y.T., Gonzalez, W.D., and Tang, F.: 1992, *Geophys. Res. Lett.* **19**, 73.
Van Ballegooijen, A.A. and Martens, P.C.H.: 1989, *Astrophys. J.* **343**, 971.
Welsch, B.T.: 2006, *Astrophys. J.* **638**, 1101.
Wilson, R.M. and Hildner, E.: 1984, *Solar Phys.* **91**, 169.
Yurchyshyn, V.B., Wang, H., Goode, P. R., and Deng, Y.: 2001, *Astrophys. J.* **563**, 381.
Yurchyshyn, V., Wang, H., Abramenko, V., Spirock, T.J., and Krucker, S.: 2004, *Astrophys. J.* **605**, 546.
Yurchyshyn, V., Hu, Q., and Abramenko, V.: 2005, *Space Weather*, **3**, S08C02, DOI: 10.1029/2004 SW000124.
Yurchyshyn, V., Karlickỳ, M., Hu, Q., and Wang, H.: 2006, *Solar Phys.* **235**, 147.
Zhao, X.P. and Hoeksema, T.J.: 1998, *J. Geophys. Res.* **103**, 2077.